Microfluid Nanofluid (2008) 5:33–41
DOI 10.1007/s10404-007-0214-z

RESEARCH PAPER

Dynamics of rotating paramagnetic particle chains simulated by particle dynamics, Stokesian dynamics and lattice Boltzmann methods

S. Krishnamurthy · A. Yadav · P. E. Phelan · R. Calhoun · A. K. Vuppu · A. A. Garcia · M. A. Hayes

Received: 1 April 2007 / Accepted: 28 July 2007 / Published online: 28 August 2007
© Springer-Verlag 2007

Abstract Paramagnetic particles, when subjected to external unidirectional rotating magnetic fields, form chains which rotate along with the magnetic field. In this paper three simulation methods, particle dynamics (PD), Stokesian dynamics (SD) and lattice Boltzmann (LB) methods, are used to study the dynamics of these rotating chains. SD simulations with two different levels of approximations—additivity of forces (AF) and additivity of velocities (AV)—for hydrodynamic interactions have been carried out. The effect of hydrodynamic interactions between paramagnetic particles under the effect of a rotating magnetic field is analyzed by comparing the LB and SD simulations, both of which include hydrodynamic interactions, with PD simulations in which hydrodynamic interactions are neglected. It was determined that for macroscopically observable properties like average chain length as a function of Mason number, reasonable agreement is found between all the three methods. For microscopic properties like the force distribution on each particle along the chain, inclusion of hydrodynamic interaction becomes important to understand the underlying physics of chain formation.

Keywords Magnetorheological fluids · Simulation · Biochemical sensors

List of symbols

A	specified constant in excluded volume force (no unit)
a	radius of particle (m)
$\mathbf{a}_{ij}$	Mobility tensor relating the linear velocity of a particle to the hydrodynamic force on a particle
$\mathbf{A}_{ij}$	Resistance tensor relating hydrodynamic force on a particle to the linear velocity of a particle
$\tilde{\mathbf{b}}_{ij}$	Mobility tensor relating the linear velocity of a particle to the hydrodynamic torque of a particle
$\tilde{\mathbf{b}}_{ij}$	Resistance tensor relating the hydrodynamic force on a particle to the angular velocity of a particle
$\mathbf{c}_{ij}$	Mobility tensor relating the angular velocity of a particle to the hydrodynamic torque of a particle
$\mathbf{C}_{ij}$	Resistance tensor relating the hydrodynamic torque to the angular velocity of a particle
d	magnitude of center-to-center distance of two particles (m)
$\mathbf{F}_i^{ev}$	excluded volume force on the ith particle (N)
$\mathbf{F}_i^{h}$	hydrodynamic force on the ith particle (N)
$\mathbf{F}_i^{m}$	magnetic force on the ith particle (N)
M	magnetization of a particle (A m^{-1})
Ma	Mason number, $Ma = \frac{12^2\eta\omega}{\mu_0 M^2}$ (no unit)
m	mass of a particle (kg)
$\hat{\mathbf{m}}$	direction of magnetic field (no unit)
$\mathbf{M}$	mobility matrix

Any opinion, findings and conclusions or recommendations expressed in this material are those of the authors and do not necessarily reflect the views of the National Science Foundation.

S. Krishnamurthy · A. Yadav · P. E. Phelan · R. Calhoun
Department of Mechanical and Aerospace Engineering,
Arizona State University, Tempe, AZ 85287-6106, USA

P. E. Phelan (✉)
The National Center of Excellence on SMART Innovations for Urban Climate + Energy, Arizona State University,
Tempe, AZ 85287-6106, USA
e-mail: phelan@asu.edu

A. K. Vuppu · A. A. Garcia
Harrington Department of Bioengineering,
Arizona State University, Tempe, AZ 85287-6106, USA

M. A. Hayes
Department of Chemistry and Biochemistry,
Arizona State University, Tempe, AZ 85287-6106, USA

$\mathbf{R}$	resistance matrix
Re	Reynolds number, $Re = \frac{\omega a^2}{\upsilon}$ (no unit)
$\mathbf{r}_{ij}$	distance between the ith and jth particles (m)
t	time (s)
$\mathbf{U}^{\infty}$	velocity of fluid (m s^{-1})
$\mathbf{v_i}$	velocity of the ith particle (m s^{-1})
$\Delta\mathbf{r}$	displacement of a particle
Δt	time step (s)
η	shear viscosity of fluid (Pa s)
μ	dipole moment of a paramagnetic particle (A m^{-2})
μ_0	permeability of free space (N A^{-2})
$\mathbf{\Omega}(t)$	angular velocity of a particle at time t (rad s^{-1})
ω	angular velocity of the rotating magnetic field (rad s^{-1})
ξ	specified constant in excluded volume force (no unit)

1 Introduction

Magneto-rheological (MR) fluids can be defined as a class of fluids in which micron-sized paramagnetic particles are suspended in a fluid such as water. Under the application of a magnetic field they form a variety of structures like columns or chains, depending on various factors like volume fraction, direction and magnitude of magnetic field, shear rates, etc. (Vuppu et al. 2003; Melle et al. 2003). They have been widely used for rheological purposes in the past because of their field-controllable effective viscosities and yield stresses (Larson 1999). More recently these MR fluids have been finding applications in new methods of sensing techniques for biochemical detection. A number of investigations in recent years have pursued the development of miniaturized devices for detecting biochemical agents (Vuppu et al. 2003, 2004). Under the influence of a rotating magnetic field, paramagnetic particles aggregate to form chains that rotate with the magnetic field. On varying the frequency of rotation or the strength of the magnetic field, the lengths of the resulting chains can be controlled. Coupled with lock-in amplification, such rotating magnetic chains can form the basis for highly sensitive biochemical detectors (Vuppu et al. 2004).

The dynamics of these fluids under various conditions are still not completely understood, and more powerful dynamic simulation tools are required for their successful application to a variety of situations. Although there have been many previous simulations of MR fluids (Martin 2001; Melle et al. 2003; Yadav et al. 2006), most of these studies employed a simplified approach to the modeling of fluid flow (such as neglecting hydrodynamic interactions between particles), and a simple Stokes drag was used to calculate the velocities. This approach is referred to here as the *particle dynamics* (PD) method. For a detailed analysis, the reader can refer to Martin (2001), Melle et al. (2003), and Yadav et al. (2006).

Prior investigations by Parthasarathy et al. (1999) have reported quantitative but no qualitative difference in the dynamic response of the dimensionless storage modulus of electro-rheological (ER) suspensions (i.e. the electrical counterparts of MR suspensions) under oscillatory shear conditions based on simulations with and without hydrodynamic interactions. Further investigations (Yadav et al. 2004, 2006) using Lattice Boltzmann simulations (LB) on the effect of hydrodynamic interaction on the dynamics of paramagnetic particles under the influence of rotating magnetic field have revealed that neglecting such interactions does not affect macroscopic quantities, but does affect microscopic quantities like the detailed forces acting on the particles. In the present study, this investigation is taken a step further by comparing the results obtained from LB simulations (Yadav et al. 2004, 2006) with those from the Stokesian dynamics (SD) method, and with the simpler PD approach. To our knowledge, this is the first comprehensive comparison of all three methods—of varying complexity—reported for the simulation of rotating paramagnetic chains.

In a real colloidal solution, the motion of the particles is governed by multi-body hydrodynamic interactions, which are taken into account by the SD method. The hydrodynamic interaction is considered by a pairwise additive scheme which can be carried out in two different ways. One method entails superposing the forces (pairwise additivity in the resistance matrix) (Bossis and Brady 1984, 1988; Brady and Bossis 1985; Durlofsky et al. 1987), and the second method entails superposing the velocity disturbances (pairwise additivity in the mobility matrix) (Satoh 2003; Satoh 2001). Though the former method reproduces the lubrication effect accurately, its application is limited to small systems as this method involves calculating the inverse of the resistance matrix. In contrast, although the additivity of the velocities is inferior in replicating the lubrication effect, it does not involve inverting the resistance matrix, thus making it applicable to large systems. In this paper both of the above-mentioned methods are used to simulate the dynamics of chains, and the results obtained are compared with those obtained from LB and PD simulations.

2 Model and simulation method

The governing equation of motion for paramagnetic particles is the Langevin equation (Yadav et al. 2004, 2006; and references cited therein):

$$m\frac{d^2\mathbf{r}_i}{dt^2} = \mathbf{F}_i^h + \mathbf{F}_i^m + \mathbf{F}_i^{\mathrm{ev}} + \mathbf{F}_i^{\mathrm{wall}} + \mathbf{F}_i^b \qquad (1)$$

where m is the particle mass, $\mathbf{r}_i$ the position of the ith particle, $\mathbf{F}_i^h$ the hydrodynamic force, $\mathbf{F}_i^m$ the magnetic force,

$\mathbf{F}_i^{\text{ev}}$ the excluded-volume force, $\mathbf{F}_i^{\text{wall}}$ the repulsive force, or the excluded-volume force between the particle and the wall, and $\mathbf{F}_i^b$ the random Brownian force. Since the magnetic force is predominant in the present simulation, the Brownian force can be neglected, and it has been assumed that the particles exist in an infinite fluid which leads to neglecting wall interaction forces. Furthermore neglecting the inertia of the particles, Eq. (1) reduces to

$$\mathbf{F}_i^h + \mathbf{F}_i^m + \mathbf{F}_i^{\text{ev}} = 0 \tag{2}$$

The expression for the magnetic force $\mathbf{F}_i^m$, assuming each particle behaves like a point dipole, is given by (Melle et al. 2003; Yadav et al. 2006; Ginder 1994):

$$\mathbf{F}_i^m = \frac{\mu_0}{4\pi} 3\mu^2 \sum_{\substack{j=1 \\ j\neq i}}^{N} \frac{1}{r_{ij}^4}\left[\left(1 - 5\left(\hat{\mathbf{m}}\cdot\hat{\mathbf{r}}_{ij}\right)^2\right)\hat{\mathbf{r}}_{ij} + 2\left(\hat{\mathbf{m}}\cdot\hat{\mathbf{r}}_{ij}\right)\hat{\mathbf{m}}\right] \tag{3}$$

where μ is the dipole moment, μ_0 the permeability of free space, $\hat{\mathbf{m}}$ the direction of the magnetic field, and $\mathbf{r}_{ij}$ the distance between the ith and jth particles. The expression for the excluded volume force $\mathbf{F}_i^{\text{ev}}$ is given as (Melle et al. 2003):

$$\mathbf{F}_i^{ev} = A\frac{3\mu_0 m^2}{4\pi(2a)^4} \sum_{\substack{j=1 \\ j\neq i}}^{N} \hat{\mathbf{r}}_{ij} \exp\left[-\xi\left(r_{ij}/2a - 1\right)\right] \tag{4}$$

where a is the particle radius, and $A = 2$ and $\xi = 10$ are specified constants. A is chosen in order to give zero interaction force when two particles, aligned along the field direction and interacting via a dipolar force, are in contact. With $\xi = 10$, the ratio between the dipolar and excluded-volume forces of two particles aligned with the field reaches the value 10 when the distance between the particles increases to $r_{ij}/2a = 1.1$. For details regarding the LB and PD simulations, the reader is referred to Yadav et al. (2004, 2006).

2.1 Modeling hydrodynamic forces

One of the most common and simplest methods of modeling the hydrodynamic force is the Stokes drag, which assumes that each particle is moving in an infinite fluid with a constant velocity:

$$\mathbf{F}_i^h = -6\pi\eta a\mathbf{v}_i \tag{5}$$

where $\mathbf{F}_i^h$ is the hydrodynamic force on the ith particle, η the shear velocity of the fluid, and $\mathbf{v}_i$ the velocity of the ith particle. While this method is simple, it neglects the hydrodynamic interactions between the particles. In other words, the motion of a particle is independent of the motion of other particles. Stokesian dynamics is an extension of the particle dynamics method where the dependence of the motion of particles on one another is taken into account at two different levels of approximation, *additivity of velocities* (AV) and *additivity of forces* (AF).

2.2 Additivity of forces

In the additivity of forces (AF) method, the forces acting on the particles are superposed in a pairwise additive method to form a resistance matrix.

In the absence of shear flow, the force $\mathbf{F}_i$ and torque $\mathbf{T}_i$ exerted on the ambient fluid flowing with a velocity of $\mathbf{U}_\infty$, by a particle i, is given by (Satoh 2003),

$$\begin{aligned}\mathbf{F}_i =& 6\pi\eta a(\mathbf{v_i} - \mathbf{U}_\infty) \\ &+ \eta\left\{\begin{array}{l}(N-1)(\mathbf{A_{ii}} - 6\pi a\mathbf{I})\cdot(\mathbf{v_i} - \mathbf{U}_\infty) \\ \quad + \sum_{j=1(\neq i)}^{N} \mathbf{A_{ij}}\cdot(\mathbf{v_j} - \mathbf{U}_\infty) \\ + (N-1)\left(\tilde{\mathbf{B}}_{\mathbf{ii}}\cdot(\mathbf{w_i} - \Omega)\right) \\ \quad + \sum_{j=1(\neq i)}^{N} \tilde{\mathbf{B}}_{\mathbf{ij}}\cdot(\mathbf{w_j} - \Omega)\end{array}\right\}\end{aligned} \tag{6}$$

$$\begin{aligned}\mathbf{T}_i =& 8\pi\eta a^3(\mathbf{w_i} - \mathbf{U}_\infty) \\ &+ \eta\left\{\begin{array}{l}(N-1)(\mathbf{B_{ii}}\cdot(\mathbf{v_i} - \mathbf{U}_\infty) + \sum_{j=1(\neq i)}^{N} \mathbf{B_{ij}}\cdot(\mathbf{v_j} - \mathbf{U}_\infty) \\ +(N-1)(\mathbf{C_{ii}} - 8\pi a^3\mathbf{I})\cdot(\mathbf{w_i} - \Omega) + \sum_{j=1(\neq i)}^{N} \mathbf{C_{ij}}\cdot(\mathbf{w_j} - \Omega)\end{array}\right\}\end{aligned} \tag{7}$$

where $\mathbf{I}$ is the unit tensor, $\mathbf{A}_{ij}$, $\mathbf{B}_{ij}$ and $\mathbf{C}_{ij}$ are the resistance tensors which are configuration dependent and taken from Kim and Karilla (1991), and $\mathbf{v}_i$, $\mathbf{w}_i$ are the translational velocity and angular velocity of the ith particle. Writing the above two equations for every particle, a matrix can be formed as (Satoh 2003; Brady and Bossis 1985):

$$\mathbf{F}_h = \mathbf{R} \cdot \mathbf{U} \tag{8}$$

where $\mathbf{F}_h$ describes the column vector containing the forces and torques (6N × 1 vector), $\mathbf{U}$ describes the column vector (6N × 1 vector) containing the translational and angular velocities of all N particles, and $\mathbf{R}$ is the resistance matrix (6N × 6N). In order to make the simulation faster, it has been assumed that the particles are subjected to high magnetic fields, and thus the torque exerted by the particles on the fluid can be assumed to be zero, i.e. the particles do not rotate about their center as they are subjected to high magnetic field. Thus neglecting the torque and the angular velocities, the resistance matrix relating the translational velocity (3N × 1) to translational force (3N × 1) reduces to a (3N × 3N) matrix. Since the magnetic and excluded volume forces are known, $\mathbf{U}$ can be solved by calculating the inverse of the resistant matrix from where the displacement of the particle can also be determined (Satoh 2003):

$$\mathbf{U} = \mathbf{R}^{-1} \cdot (\mathbf{F}_m + \mathbf{F}_{\mathrm{ev}}) \tag{9}$$

$$\Delta\mathbf{r} = \left[\mathbf{R}^{-1}(\mathbf{F}_m + \mathbf{F}_{\mathrm{ev}})\right]\Delta t \tag{10}$$

Thus for a system of N particles the simulation requires inverting the 3N × 3N resistance matrix at every time step. Since the scalar functions used in the present method have been obtained using the boundary collocation method (Kim and Karilla 1991), in which the lubrication effects have been well accounted for, the present method is capable of replicating the physics of the particles motion accurately. Furthermore in this method the pair interactions appear indirectly as multi-body hydrodynamic interactions through the inverse procedure of the resistance matrix (Durlofsky et al. 1987), which makes it a dynamic method for simulating such systems.

2.3 Additivity of velocity

Following the same procedure as shown above for the additivity of forces, the equation for the velocity of particle i, $\mathbf{v}_i$, can be written in a pairwise additive method to form the mobility matrix. In the absence of a shear flow, $\mathbf{v}_i$ and the angular velocity $\mathbf{w}_i$ of a particle are written as (Satoh 2003):

$$\mathbf{v_i} = \frac{1}{\eta}\left\{\begin{array}{l} \dfrac{1}{6\pi a}\mathbf{F_i} + (N-1)(\mathbf{a_{ii}} - \dfrac{1}{6\pi a}\mathbf{I}) \cdot \mathbf{F}_i \\ \displaystyle\sum_{j=1(\neq i)}^{N} \mathbf{a_{ij}} \cdot \mathbf{F_j} + (N-1)\tilde{\mathbf{b}}_{\mathbf{ii}} \cdot \mathbf{T}_i + \sum_{j=1(\neq i)}^{N} \tilde{\mathbf{b}}_{\mathbf{ij}} \cdot \mathbf{T_j} \end{array}\right\} \tag{11}$$

$$\mathbf{w_i} = \frac{1}{\eta}\left\{\begin{array}{l} \dfrac{1}{8\pi a^3}\mathbf{T_i} + (N-1)\tilde{\mathbf{b}}_{\mathbf{ii}} \cdot \mathbf{F_i} + \displaystyle\sum_{j=1(\neq i)}^{N} \tilde{\mathbf{b}}_{\mathbf{ij}} \cdot \mathbf{F_j} + \\ (N-1)(\mathbf{c_{ii}} - \dfrac{1}{8\pi a^3}\mathbf{I}) \cdot \mathbf{T_i} + \displaystyle\sum_{j=1(\neq i)}^{N} \mathbf{c_{ij}} \cdot \mathbf{T_j} \end{array}\right\} \tag{12}$$

where $\mathbf{a}_{ij}$, $\mathbf{b}_{ij}$ and $\mathbf{c}_{ij}$ are the mobility tensors, which are again configuration dependent and taken from (Durlofsky et al. 1987; Kim and Karilla 1991). Making the same assumption as that in the AF method for neglecting the torque and angular velocities, the translational velocities of the particles and hence the displacement can be found by multiplying the mobility matrix 3N × 3N with the force vector 3N × 1 as shown below,

$$\mathbf{U} = \mathbf{M}(\mathbf{F}_m + \mathbf{F}_{ev}) \tag{13}$$

$$\Delta\mathbf{r} = [\mathbf{M}(\mathbf{F}_m + \mathbf{F}_{\mathrm{ev}})]\Delta t \tag{14}$$

Importantly, the AV approach does not require the inversion of a matrix Eqs. (9) and (10), while the AF approach does (Eqs. (13) and (14)).

2.3.1 *Lattice Boltzmann method*

In the lattice Boltzmann method the hydrodynamic force on the particles is calculated by summing up the forces on all the boundary nodes (Ladd and Verberg 2001). At each of the boundary nodes the hydrodynamic force can be calculated using Eq. 15:

$$\mathbf{f_i}\left(\mathbf{r}_b, t + \frac{\Delta t}{2}\right) = \frac{\Delta x^3}{\Delta t}\left(2n_b^*(\mathbf{r}, t) - \frac{2a^{c_b}\rho_0\mathbf{u}_b \cdot \mathbf{c}_b}{c_s^2}\right)c_b \tag{15}$$

where $\mathbf{f}_i$ is the hydrodynamic force on one boundary node of the ith particle, $\mathbf{r}_b$ the position vector of the boundary node, Δx and Δt the lattice spacing and time step respectively, n_b^* (r,t) the postcollision distribution at $(\mathbf{r}, t)$, ρ_0 the equilibrium fluid density, $\mathbf{u}_b$ the velocity at particle surface $\mathbf{r}_b$, satisfying the stick boundary conditions, $\mathbf{c}_b$ the lattice velocity vector of the boundary node, a^{c_b} a constant depending on the type of lattice, and c_s the speed of sound in the fluid. The total force and torque on the ith particle can be calculated by summing the forces and torques on each individual node as given below:

$$\mathbf{F_i^h} = \sum \mathbf{f_i}(\mathbf{r}_b, t)$$
$$\mathbf{T_i^h} = \sum \mathbf{r}_b \times \mathbf{f_i}(\mathbf{r}_b, t) \quad (16)$$

Since the momentum space of the fluid in the lattice Boltzmann method is discrete, it is not possible to match the velocity of the fluid at the boundary to that of the solid by directly equating the velocities of the fluid and surface at the boundary nodes. But if the distribution function at the boundary node is modified in such a way that the momentum transfer to the particle is the same as in the case of a no-slip boundary condition then we can implement the no-slip boundary condition. This method results in a small amount of fluid flowing in or out of each boundary node so that there is a redistribution of fluid mass across the boundary nodes. The additional mass which is added to or removed from the particle is exactly recovered when the particle is moved to its new position in the next timestep.

2.4 Nondimensional parameters

A nondimensional parameter which gives the ratio of magnetic and viscous forces on the particles is the Mason number (*Ma*). It is used in this work to characterize the strength of viscous and magnetic forces. It is derived by non-dimensionalizing the Langevin equation (Eq. (1)) with respect to time and distance, upon which a non-dimensional time, τ, is defined:

$$\tau = \frac{12^2\eta}{\mu_0\mu_s M^2} \quad (17)$$

This timescale τ, which when multiplied by ω (the angular frequency of rotation of the magnetic field) gives the Mason number *Ma*:

$$Ma = \frac{12^2\eta\omega}{\mu_0 M^2} \quad (18)$$

where M is the magnetization of the paramagnetic particles, η the viscosity of the fluid, ω the rotational frequency of the magnetic field and μ_o the permeability of free space. M is related to the induced dipole moment, μ, of the particles by:

$$\mu = \frac{4}{3}\pi a^3 M \quad (19)$$

where a is the radius of the particle. Since the magnetization of these particles has been found to saturate at higher magnetic fields (Melle et al. 2002), it can be assumed that the induced dipole moment is constant and doesnot vary with magnetic field. The Mason number gives the ratio of viscous force magnitude and (magnetic) + (excluded volume force) magnitude when only two particles are present. In order to avoid the particles from overlapping in this analysis, an excluded volume force is also considered. The timescale τ can be thought of as the time required for a particle to move under the influence of another polarized particle. The time ω^{-1} can be considered as the shearing time for a particle moving with angular frequency ω. If τ is greater then ω^{-1} (or Mason number > 1), then the time for shearing of a particle is less than the time for the particle to move under the influence of a magnetic field, and hence no stable chains will form as will be shown later in the Sect. 3. The Reynolds number, *Re*, for the particles is calculated from:

$$Re = \frac{\omega a^2}{\upsilon} \quad (20)$$

2.5 Computer simulations

Two types of SD simulations, namely additivity of forces (AF) and additivity of velocities (AV), were carried out to study the dynamics of chains of paramagnetic particles. Both of the above-mentioned simulation methods were applied to a box of size $200 \times 200 \times 200$ (in μm). Periodic boundary conditions were applied in all three directions and in order to obtain results quickly, all the particles were placed in the *XY* plane. The frequency of the rotating magnetic field was set to 1 Hz so that the system is in the low *Re* regime. The magnitude of *Ma* was changed by varying the parameters in the *Ma* definition given in Eq. (16), but keeping ω constant. The scalar functions required for including the hydrodynamic interactions between the particles were tabulated as functions of particle–particle separation using the numerical scheme suggested by Kim and Mifflin (1991). A suitable interpolation scheme was used to obtain the scalar functions for arbitrary separation from these tabulated values. These scalar functions are singular in nature, i.e., as the particle–particle separation increases, the values of the scalar functions increase rapidly. In order to ensure the program doesn't stop as a result of this singularity, the resistance functions are assumed to vary linearly between $d = 2.001$ and $d = 2$ where d is the nondimensional particle–particle separation ($r/2a$).

The PD and LB simulations are described in detail elsewhere (Yadav et al. 2004, 2006), and so are not repeated here.

3 Results and discussion

Figure 1 shows the variation of chain length as a function of *Ma*. The chain length has been non-dimensionalized

with the diameter of the particle. At low *Ma*, the magnetic forces acting on the particles dominate over the viscous forces as a result of which the particles aggregate to form chains. Thus as *Ma* increases, the magnetic forces acting on the particles tend to decrease which, has the effect of forming smaller-length chains. This variation can be clearly noticed in Fig. 1. Though all the simulation methods predict similar chain lengths for varying *Ma*, they do not agree with the experimental results obtained from Melle et al. (2002a) and Vuppu et al. (2003), which in fact disagree with each other in magnitude, but not in trend. The reason for the mismatch between the experimental and simulation results can be attributed at present to two different factors, the presence of surface groups on the particles in the experiments whose effect is not simulated in the current problem, and the assumption of the saturation of the magnetization of the particles. In reality the saturation occurs non-uniformly around the particle, which can affect the magnetic interaction force existing between the particles.

As mentioned above, a possible reason for the discrepancy between the results obtained from Melle et al. (2002a) and Vuppu et al. (2003) could be because of using particles with different surface groups. While in Melle et al.'s experiments (2002a, b) carboxylic groups were attached to the paramagnetic particles, in Vuppu et al.'s experiments (2003) amine-functionalized paramagnetic particles were used. Another particularly important difference between the two experiments was the presence (or absence) of a surfactant. Melle et al. (2002a) used paramagnetic beads that were not only initially coated with surfactant, but in fact additional surfactant was added to the solution. On the contrary, Vuppu et al. (2003) removed all traces of surfactant from their solution containing the paramagnetic particles. The chemistry of the solution, such as the pH value, the type of base fluid (aqueous or organic), and the aging of solution, will also likely influence the chain formation. The trend of the variation for the simulations and experimental results, however, are identical. The average slope of the lines for LB, AF and PD simulations is 0.5, which is in agreement with that measured in experiments by Melle et al. (2002a) from a chain length versus ω plot (Melle et al. 2002b, 2003).

Figure 1 shows that the results for chain lengths from the PD simulations are in excellent agreement with those from the more comprehensive LB and SD simulations. This is despite the fact that in the PD simulations, the near-field and far-field hydrodynamic interactions are neglected. In order to understand this phenomenon more deeply, a comprehensive force analysis was performed. A case where the domain consisted of 9 particles was considered and the force distribution on each of these particles when they form a chain and rotate with the magnetic field was investigated. The simulation for this case was run at a low *Ma* of 0.015 to facilitate chain formation, and the results obtained from all four simulation methods are shown in Fig. 2. Figure 3 shows the snap shots of these aggregates for two extreme Mason numbers.

Figure 2 presents the total force experienced by the particles in the direction of their motion, or in other words, the total drag force experienced by the particles. The forces are non-dimensionalized by the Stokes drag on a 2-particle chain rotating about its axis, which is given by $6\pi\eta a(\omega a)$. The actual hydrodynamic force will

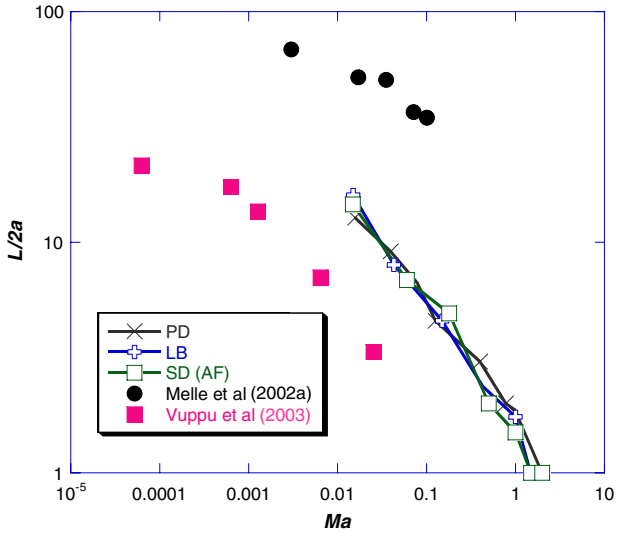

Fig. 1 Comparison of the variation of chain length with *Ma* from simulations with experimental data from Vuppu et al. (2003) and Melle et al. (2002a)

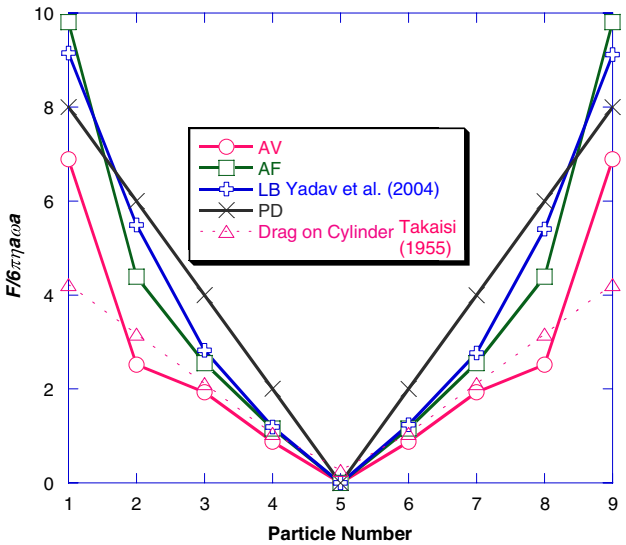

Fig. 2 Comparison of drag forces acting on the particles from simulations

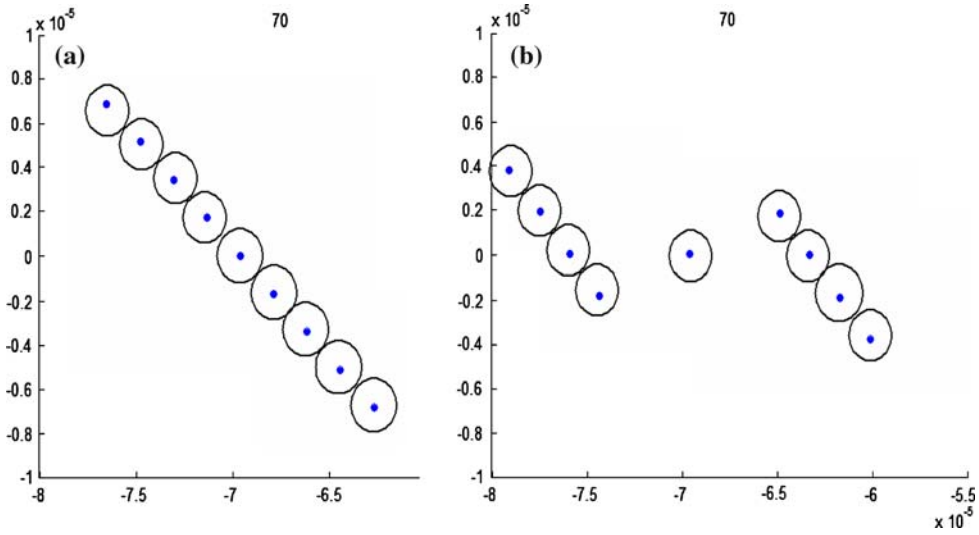

Fig. 3 Chain Formation at **a** $Ma = 0.015$ and **b** $Ma = 0.15$

be much larger than this tangential component of the total force. From Fig. 2 it is observed that for the AF and LB simulations, the force distribution is nearly identical, with the particles in the periphery subjected to a maximum force slightly greater than the Stokes drag, and the particles in the center being subjected to forces slightly lower than the Stokes drag. This reduction of forces can be attributed to the shielding effect wherein the particle interaction is shielded as a result of the presence of an intervening third particle. But the drag force experienced by the particles for the AV simulation is comparatively less than that of the Stokes drag. This is because the mobility formulation (AV) is based on a point-force approximation. When two particles come close to each other, the surfaces of the two spheres tend to squeeze out all the fluid between them, which results in high-pressure forces between the two spheres. This effect is termed as the lubrication effect, and is an important parameter for simulating physically accurate systems. When a point-force approximation is made in the mobility formulation, we are not able to capture the dominant lubrication effect; as a result the total hydrodynamic forces simulated by this method are much lower than that obtained from LB and AF simulations. Thus the AV method is inferior to the AF method in reproducing the lubrication effect.

Since the drag forces acting on the particles are identical for the AF, LB and PD simulations, the predicted chain lengths are similar for each of these methods. This validates that Stokes drag is a very good approximation for computing the drag force acting on the particles in a rotating chain. The drag force calculated on a cylinder according to Takaisi (1955) has also been plotted in Fig. 2. As expected, it is much less than the Stokes drag, and shows that the chain does not behave like a cylinder rotating about its axis, although intuitively one might think so. The higher drag force experienced by the particles in a chain is due to the large hydrodynamic forces acting on the particles in the chain. As a result the tangential component of this force (drag force) is much higher than the drag experienced by the cylinder.

The next question which arises as a result of the above discussion is that if the hydrodynamic forces are neglected in a PD simulation, how does one account for the balance between the magnetic and excluded volume forces? Detailed discussion on this front has been covered in Yadav et al. (2004, 2006); here this issue will be discussed qualitatively. The excluded volume forces used in the present simulations increases exponentially with a decrease in the separation distance between the particles, as a result preventing the particles from overlapping with each other. But since this force is short range in nature (exponential function), its main contribution is from particles close to it and contributions from far-field particles diminish with increasing distance. On the other hand the magnetic force is still a long-range force with contributions from far-field particles. Thus in PD simulations, there is a slight (3%) overlap between the particles which is evident in Fig. 4 where the distance between neighboring particles (i.e. the distance between particles 1 & 2, 2 & 3,…,8 & 9) is plotted versus the particle number of the first particle (1, 2,…,8). Since the overlap is relatively small, the chain lengths do not change appreciably. Figure 4 also shows that there is overlap between the particles in the AV formulation, with again the reason for this being that the AV formulation is inferior to the other methods (LB and AF) in simulating the lubrication effect. On the other hand, the LB and AF simulations are able to simulate the lubrication effect effectively, as the particles do not overlap in these methods.

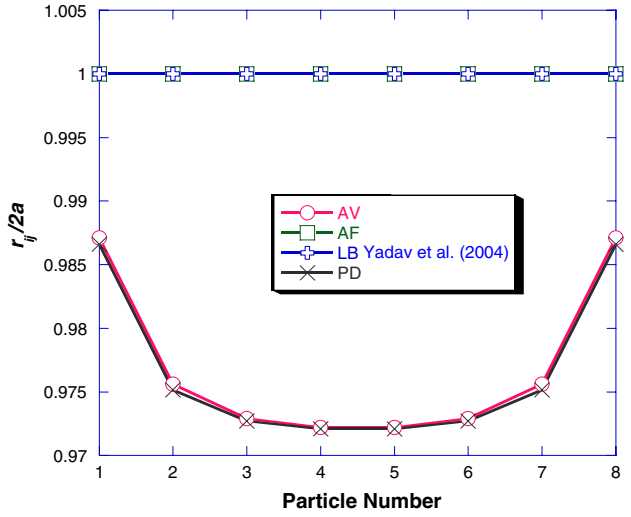

Fig. 4 Comparison of distance between adjacent particles from simulations

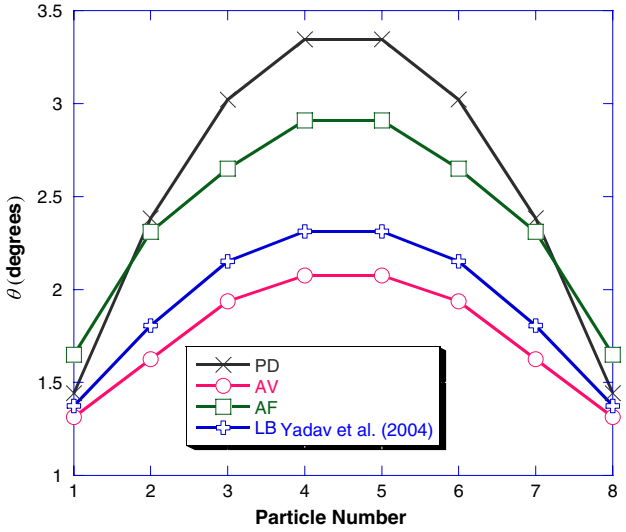

Fig. 5 Comparison of phase difference computed from different simulations

Due to the presence of the fluid, the paramagnetic chain will lag the magnetic field. Figure 5 shows the variation of this phase difference of neighboring particles with magnetic field as a function of particle number for the AF, AV, LB and PD simulations. It can be seen from the graph that the phase difference is higher at the center of the chain than that observed at the outer edges of the chain. This is as a result of the higher drag force acting on the particles at the periphery evident in Fig. 2. This has the effect of dragging the particles in the opposite direction of their motion, as a result of which a larger phase angle is observed in the center. The phase angle for the particles at the periphery for the AF simulations is found to be more than the phase angle for Stokes drag. This can be attributed to the fact that the drag force acting on these particles is greater than the Stokes drag. It can be noticed that the phase angle varies along the length of the chain. This information on phase angle can be used to predict the shape of the rotating chain, which is S-shaped in this case. The phase lag for the AV method is lower than that observed from the AF method, because the drag force predicted by the AV method is less than other methods as is evident in Fig. 2.

Finally, Fig. 6 presents the variation of chain phase lag with *Ma* for the PD and AF simulations. To calculate the chain phase lag, we follow the method implemented by Melle et al. (2002a, b), where the averaged chain phase lag distribution is weighted by the chain size:

$$\theta = \frac{\sum_j N_j \theta_j}{N_a} \tag{21}$$

where N_a is the number of aggregated particles, θ_j the phase angle of the jth chain, and the sum is done over j with $N_j > 1$. As *Ma* increases, the phase angle increases, and the viscous forces start dominating over magnetic forces, which results in long chains breaking into shorter chains. During this breakup, the phase angle increases. As *Ma* is increased, this phenomenon occurs more frequently, resulting in the increase in phase angle ultimately saturating once all the chains are broken. It can be further noticed that the chain phase lag for the AF simulation is less than that obtained from the PD simulation, which is due to the drag experienced by particles in AF simulations being less than the Stokes drag. This difference reduces with an increase in *Ma* because shorter chains are formed at higher *Ma*, and as a result the drag force experienced by these

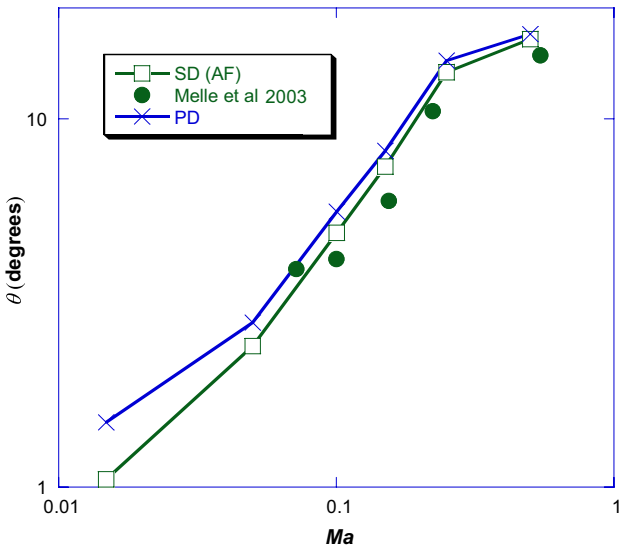

Fig. 6 Comparison of chain phase lag variation with *Ma*, between simulations and experimental data

particles becomes closer to the Stokes drag. Comparison with experimental data (Melle et al. 2002b) in Fig. 6 shows better agreement with the AF simulations compared to the PD simulations.

The quantitative comparisons among the three computational approaches for predicting the dynamics of rotating chains of paramagnetic particles—particle dynamics, a complete Navier–Stokes solution including two-way coupling between the particles and the fluid based on the lattice-Boltzmann approach, and Stokesian dynamics—reveals that in large part the simplest method, particle dynamics, is able to predict the relatively gross dynamics of the particle chains with acceptable accuracy. For detailed computations of finer details, such as the angle between particles or (to a lesser extent) the phase lag between a particle chain and the rotating magnetic field, the more numerically intensive computational approaches are required.

4 Conclusions

The dynamics of rotating paramagnetic particle chains using three different levels of approximation are quantitatively compared. It is observed that all three methods—particle dynamics (PD), Stokesian dynamics (SD), and lattice Boltzmann (LB)—capture the dynamics of the rotating chain effectively. While the SD and LB methods take into account the important hydrodynamic interactions between particles, the PD method neglects these interactions. Despite this assumption, it is found that the macroscopic chain dynamics is predicted rather accurately by the comparatively simple PD method. On comparing the forces acting on the particles using the three simulation methods, it was found that the Stokes drag is a good approximation for the drag acting on these particles. The results showing the variation of chain length with Mason number, *Ma*, for each of these methods validate this assumption. But the differences in drag forces acting on these particles in each of these methods has been shown to affect the phase angle between the particles. The variation of phase lag with Mason number suggests that accounting for hydrodynamic interaction predicts the phase angle more accurately. While the particles do not overlap in the LB and SD simulations due to the inclusion of the hydrodynamic interactions in these methods, in the PD method, the particles do in fact overlap hydrodynamic interaction is neglected. The excluded volume forces compensate for the absence of normal hydrodynamic forces in the PD simulations, and cause overlap between particles. But avoiding the calculation of hydrodynamic force, makes this method the fastest among the other methods investigated in this paper. Hence, particle dynamics is able to predict the dynamics of the chain formation effectively despite the fact that it neglects the important hydrodynamic interactions.

Acknowledgment The authors gratefully acknowledge the support of the National Science Foundation, through a Nanoscale Exploratory Research (NER) grant (Award Number 0303883). This material was based in part on work supported by the National Science Foundation, while working at the Foundation. The authors would also like to thank Dr. A.J.C. Ladd for helpful discussions and providing his LB code.

References

Bosis G, Brady JF (1984) Dynamic simulation of sheared suspensions. 1 General method. J Chem Phys 80:5141

Brady JF, Bossis G (1985) The rheology of concentrated suspensions of spheres in simple shear flow by numerical simulations. J Fluid Mech 155:105

Brady JF, Bossis G (1988) Stokesian dynamics. Annu Rev Fluid Mech 20:111

Durlofsky L, Brady JF, Bosis G (1987) Dynamic simulations of hydrodynamically interacting particles. J Fluid Mech 180:21

Ginder JM, Davis LC (1994) Shear stresses in magnetorheological fluids: role of magnetic saturation. Appl Phys Lett 65:3410–12

Kim S, Karilla SJ (1991) Micro hydrodynamics. Butterworth-Heinemann, Boston

Ladd AJC, Verberg R (2001) Lattice-Boltzmann simulations of particle-fluid suspensions. J Stat Phys 104:1191–1251

Larson RG (1999) The structure and rheology of complex fluids. Oxford Publications, New York

Martin JE (2001) Thermal chain model of electrorheology and magnetorheology. Phys Rev E 63:011406

Melle S, Calderòn OG, Fuller GG, Rubio MA (2002a) Polarizable particle aggregation under rotating magnetic fields using scattering dichroism. J Colloid Interface Sci 247:200

Melle S, Calderón OG, Rubio MA, Fuller GG (2002b) Rotational dynamics in dipolar colloidal suspensions: video microscopy experiments and simulations results. J Non Newtoninan Fluid Mech 102:135

Melle S, Calderón OG, Fuller GG, Rubio MA (2003) Microstructure evolution in magnetorheological suspensions governed by Mason number. Phys Rev E 68:041503

Parthasarthy M, Klingenberg DJ (1999) Large amplitude oscillatory shear of ER suspensions. J Non Newtonian Fluid Mech 81:83

Satoh A (2001) Comparison of approximations between additivity of velocities and additivity of forces for stokesian dynamics methods. J Colloid Interface Sci 243:342

Satoh A (2003) Introduction to molecular-microsimulation of colloidal dispersion. Elsevier, Amsterdam

Takaisi Y (1955) The drag on a cylinder moving with low speeds in a viscous liquid between two parallel walls. J Phys Soc Jpn 10:8

Vuppu AK, Garcia AA, Hayes MA (2003) Videomicroscopy characterization of dynamically aggregated paramagnetic micrrotors in an applied rotating magnetic field. Langmuir 19:8646

Vuppu AK, Garcia AA, Hayes MA, Booksh K, Phelan PE, Calhoun R, Saha SK (2004) Phase sensitive enhancement for biochemical detection using paramagnetic particle chains in an applied rotating magnetic field. J Appl Phys 96:6831

Yadav A, Calhoun R, Phelan PE, Vuppu AK, Garcia AA, Hayes MA (2004) Simulation of magneto-rheological fluids using lattice boltzmann method. Paper No. IMECE2004-60301. In: Proceedings of 2004 ASME international mechanical engineering congress and exposition (IMECE'04), 13–19 November, Anaheim

Yadav A, Calhoun R, Phelan PE, Vuppu AK, Garcia AA, Hayes M (2006) Dynamics of rotating paramagnetic particles simulated by lattice boltzmann and particle dynamics methods. IEE Proc Nanobiotechnol 153:145